

Ground state properties of the disordered spin-one Bose-Hubbard model: a stochastic mean-field theory study

Jesus Herazo Warnes and Eduardo Miranda

Instituto de Física Gleb Wataghin, Unicamp, Rua Sérgio Buarque de Holanda, 777, CEP 13083-859, Campinas, SP, Brazil

(Dated: March 8, 2013)

We study the ground state of the disordered Bose-Hubbard model for spin-1 particles by means of the stochastic mean-field theory. This approach enables the determination of the probability distributions of various physical quantities, such as the superfluid order parameter, the average site occupation number, the standard deviation of the occupation per site and the square of the spin operator per site. We show how a stochastic method, previously used in the study of localization, can be flexibly used to solve the relevant equations with great accuracy. We have determined the phase diagram, which exhibits three phases: the polar superfluid, the Mott insulating and the Bose glass. A complete characterization of the physical properties of these phases has been established.

PACS numbers: 67.85.Fg, 67.85.Hj, 67.85.-d

I. INTRODUCTION

Systems of cold atoms have become an enormously rich playground for the study of strongly correlated quantum matter. This era was probably heralded by the observation of the superfluid to Mott insulator phase transition in systems of ^{87}Rb loaded in optical lattices¹. Since then, the possibility of a great amount of control over the parameters of these systems has attracted the attention of both the atomic and the condensed matter physics communities².

More recently, the ability to introduce quenched disorder into the system in a controlled manner has provided researchers with yet another ‘knob’ to be turned in these studies². Disorder can be incorporated in several ways, namely, through the addition of laser speckle patterns to the optical lattice potential^{3,4}, through the creation of a quasi-random optical profile by means of different laser fields with incommensurate frequencies⁵⁻⁹, by means of randomly trapped atomic ‘impurities’^{10,11}, or even random magnetic fields close to a Feshbach resonance which can modify locally the scattering length between the atoms¹². This great flexibility holds a great deal of promise in the study of the interplay between interactions and disorder, a problem of enormous importance in condensed matter physics¹³.

One other attractive feature of cold atomic systems is the fact that they can often be very efficiently described by the simple effective models of condensed matter physics, with much better justification for the approximations made in arriving at these models. Foremost among these is the Bose-Hubbard model for spin-zero bosons, which forms the paradigm for theoretical studies¹⁴⁻¹⁶. Indeed, in the conventional magnetic traps frequently used, the internal degrees of freedom (spins) of the atoms are frozen and they can be described as spinless bosons. However, in purely optical traps the spins are liberated and the condensates formed depend crucially on the degeneracy of the atomic spinor¹⁷⁻²⁰. Again, the usual approximation of retaining only low-energy s -wave scattering between atoms justifies the description

of these systems by means of the Bose-Hubbard model generalized for particles with spin greater than or equal to one²¹.

A fairly good yet simple treatment of the spin-zero Bose-Hubbard model is afforded by the so-called ‘site-decoupled’ mean-field theory^{14,15,22}, which is able, in particular, to identify the phases of the model and the topology of the phase diagram at zero temperature. The latter exhibits (i) a superfluid (SF) phase, characterized by a macroscopic occupation of the lowest single-particle state (the $\mathbf{k} = 0$ state in the case of equilibrium)²³ or, equivalently, by the spontaneous breaking of gauge symmetry²⁴, and (ii) a series of Mott insulator (MI) lobes, each characterized by an integer occupation per site and a vanishing compressibility due to the presence of an interaction-induced gap. This is in good qualitative agreement with other more accurate methods (see, e. g., 25).

This mean-field theory was extended to the spin-1 case and used not only for the analysis of the ground state of the model^{21,26} but also for finite temperatures²⁷. In the pioneering work of reference 21, the ground state phase diagram was determined for an antiferromagnetic intra-site interaction. It was found that, although both superfluid (SF) and Mott insulating (MI) phases are found, like in the spin-zero case, in contrast to the latter there are two qualitatively different MI lobes: those with an odd number of bosons combined in a total spin 1 composite per site, and even-numbered lobes with a total spin singlet per site. Moreover, the SF phase was found to have a so-called ‘polar’ structure, corresponding to a spin-zero condensate. The presence of a non-zero spin per site can lead to a non-trivial magnetic order. Indeed, it has been proposed that the MI phases can show spin nematic order, a state with broken spin rotational symmetry but unbroken time reversal symmetry²⁸.

Although the clean Bose-Hubbard models have by now been fairly well studied, the introduction of quenched disorder poses a much more complex problem. In the ground-breaking work of reference 14, scaling arguments were used to address the zero-temperature phase diagram, the associated quantum phase transitions, and

other physical properties of the disordered spin-zero Bose-Hubbard model. Perhaps the most important conclusion of that work was the prediction of a new Bose Glass (BG) phase, which is characterized by localized, insulating behavior in the absence of an excitation gap and hence, with a finite, non-zero compressibility. Although the unbiased confirmation of the existence of this phase by numerical methods is highly non-trivial, there is by fairly good evidence in favor of it (see, e. g., 29–31).

A theoretical study of the effects of disorder in the spin-1 Bose-Hubbard model was carried out in reference 32, in which the ground state phase diagram was determined by using the Gutzwiller variational method and a mean-field theory based on the arithmetic average of the SF order parameter. For the case of diagonal disorder (i. e., randomness in the local orbital energies), it was found that the odd-numbered MI lobes are rapidly transformed into a BG regions, whereas the even-numbered ones are much more robust with respect to randomness, requiring a much larger strength of disorder before they also turn into a BG.

The ‘site-decoupled’ mean-field theory mentioned above can be readily generalized to the disordered case, although its full solution requires numerical work^{15,33}. A great deal of insight into this approach can be gained, however, through a simplification proposed in 34 and 35. It consists of directing the focus of attack towards the determination of the probability density distribution function of local SF order parameters, $P(\psi)$. After ignoring correlations among order parameters in nearby sites, the next step is to establish a mean-field self-consistent condition to be satisfied by $P(\psi)$. This method was dubbed Stochastic Mean Field Theory (SMFT) because it has an immediate formulation as a stochastic equation. The method offers some advantages over alternative approaches in that it does not suffer from finite-size effects and crucially, it allows a great deal of analytical control, specially over the probability distribution of local quantities. It does have the drawback of predicting a direct MI-SF transition at weak disorder without an intervening BG phase, which can be ruled out on firm theoretical grounds³⁶. Nevertheless, despite this shortcoming, it provides a fairly powerful tool for the analysis of these intricate disordered systems. Indeed, qualitatively the overall phase boundaries obtained within SMFT for the zero spin case agree well³⁵ with Quantum Monte Carlo results in finite lattices³⁷.

We should also mention the important analysis of the disordered spin zero boson problem afforded by the real space renormalization group appropriate for strong disorder^{38–41}, a powerful tool especially in low dimensions. It focused on a quantum rotor representation believed to be equivalent to the Bose-Hubbard Hamiltonian in the limit of a large number of bosons per site. The system was thoroughly characterized in one spatial dimension^{38–40}, which is special since there can be only quasi-long range (power-law) superfluid order in the ground state. Like the clean case, the quantum

superfluid-insulator transition belongs to the Kosterlitz-Thouless universality class. In the disordered case, however, this transition can occur at arbitrarily weak interactions, which sets it apart for its higher-dimensional counterparts. The insulating phase has the expected features (i.e. a finite compressibility) of a Bose glass for generic disorder. Other types of disorder with special particle-hole symmetry properties were also considered, in which case the insulator can have vanishing (the so-called Mott glass) or infinite compressibility (dubbed a random singlet glass). More recently, this approach has been extended to two dimensions⁴¹, in which case the transition is governed by a more conventional unstable fixed point at finite interaction strength. However, this was confined to the non-generic particle-hole symmetric disorder that does not give rise to a Bose glass phase. It should be mentioned that all fixed points found show finite effective disorder, which renders the method less conclusive than at other infinite disorder fixed points for which the method is asymptotically exact.

The aim of this paper is to analyze the disordered spin-1 Bose-Hubbard model with the tools of the SMFT^{34,35}. We will focus our attention on the antiferromagnetic interaction case only. We have found that the phase diagram of reference 32 is well captured by this simplified approach. Furthermore, we are also able to find a number of distribution functions of local quantities which offer a great deal of insight into the nature of the various phases, namely, the local spinor order parameters, the average and the standard deviation of the site occupation, and the total spin per site. Finally, by analyzing the behavior of the system both as a function of interactions and as a function of disorder strength we track the hierarchical transformation of the MI lobes into BG phases. It should be mentioned that, unlike in the original application of the SMFT^{34,35}, we use an alternative stochastic approach to solve the SMFT equations which was first suggested in reference 42 and used extensively in 43 and proves to be quite efficient and flexible.

The paper is organized as follows. In Section II, we present the model and review the phase diagram both in the clean and disordered cases. In Section III, we explain how the SMFT is defined and also describe our strategy for solving the corresponding equations. We then present our results in Section IV. We wrap up with some conclusions in Section V.

II. THE MODEL

We will focus on a generalized disordered Hubbard model for bosons with total spin $F = 1$ ²¹

$$\begin{aligned}
H = & -t \sum_{\langle i,j \rangle} \sum_{\alpha} a_{i\alpha}^{\dagger} a_{j\alpha} \\
& + \sum_i \sum_{\alpha} (\epsilon_i - \mu) a_{i\alpha}^{\dagger} a_{i\alpha} \\
& + \frac{U_0}{2} \sum_i \sum_{\alpha, \beta} a_{i\alpha}^{\dagger} a_{i\beta}^{\dagger} a_{i\beta} a_{i\alpha} \\
& + \frac{U_2}{2} \sum_i \sum_{\alpha, \beta, \gamma, \delta} a_{i\alpha}^{\dagger} a_{i\gamma}^{\dagger} \mathbf{S}_{\alpha\beta} \cdot \mathbf{S}_{\gamma\delta} a_{i\delta} a_{i\beta}, \quad (2.1)
\end{aligned}$$

where $a_{i\alpha}^{\dagger}$ creates a bosonic atom with spin projection $\alpha \in \{-1, 0, 1\}$ in an optical lattice Wannier function centered on the site i , t is a nearest-neighbor hopping amplitude, μ is the chemical potential (we will work in the grand-canonical ensemble), U_0 and U_2 are local (intra-site) coupling constants for spin-independent and spin-dependent interactions, respectively, and $\mathbf{S} = S_x \hat{\mathbf{x}} + S_y \hat{\mathbf{y}} + S_z \hat{\mathbf{z}}$ are the spin-1 matrices given by

$$\begin{aligned}
S_x = \frac{1}{\sqrt{2}} \begin{pmatrix} 0 & 1 & 0 \\ 1 & 0 & 1 \\ 0 & 1 & 0 \end{pmatrix}, \quad S_y = \frac{i}{\sqrt{2}} \begin{pmatrix} 0 & -1 & 0 \\ 1 & 0 & -1 \\ 0 & 1 & 0 \end{pmatrix}, \\
S_z = \begin{pmatrix} 1 & 0 & 0 \\ 0 & 0 & 0 \\ 0 & 0 & -1 \end{pmatrix}. \quad (2.2)
\end{aligned}$$

The interaction coupling constants can be related to the s -wave scattering lengths of two bosons in vacuum with total spin 0 (a_0) and 2 (a_2) (the symmetric nature of their wave function forbidding s -wave processes with total spin 1)²¹

$$U_0 = \frac{4\pi\hbar^2}{3M} (a_0 + 2a_2) I_4, \quad (2.3)$$

$$U_2 = \frac{4\pi\hbar^2}{3M} (a_2 - a_0) I_4, \quad (2.4)$$

where M is the boson mass and I_4 is the integral of the fourth power of the Wannier wave function. As per the usual nomenclature, the spin-dependent interaction is called ferromagnetic, when $U_2 < 0$ (i.e., $a_2 < a_0$) and antiferromagnetic if $U_2 > 0$ (i.e., $a_2 > a_0$)¹⁷. On-site disorder is introduced through the parameters ϵ_i , which are taken to be random quantities with no spatial correlations. Although several models of disorder may be considered, for simplicity we chose ϵ_i to be distributed according to a uniform distribution of width 2Δ .

It is useful to introduce the single-site operators for the total number of bosons n_i and total spin \mathbf{S}_i ,

$$\hat{n}_i = \sum_{\alpha} a_{i\alpha}^{\dagger} a_{i\alpha}, \quad (2.5)$$

$$\mathbf{S}_i = \sum_{\alpha, \beta} a_{i\alpha}^{\dagger} \mathbf{S}_{\alpha\beta} a_{i\beta}, \quad (2.6)$$

in terms of which the Hamiltonian (2.1) can be rewritten as

$$\begin{aligned}
H = & -t \sum_{\alpha} \sum_{\langle i,j \rangle} a_{i\alpha}^{\dagger} a_{j\alpha} + \frac{U_0}{2} \sum_i \hat{n}_i (\hat{n}_i - 1) \\
& + \frac{U_2}{2} \sum_i (\mathbf{S}_i^2 - 2\hat{n}_i) + \sum_i (\epsilon_i - \mu) \hat{n}_i. \quad (2.7)
\end{aligned}$$

In the clean limit, the model exhibits two phases: a superfluid phase (SF) and several lobes of Mott insulating (MI) behavior²¹. The SF is the so-called polar state, characterized by a spin-zero Bose-Einstein condensate (BEC). As any superfluid state, it can be characterized by the appearance of a non-zero value of $\langle a_{i\alpha} \rangle$ for some component α , and this situation corresponds to the spontaneous breaking of gauge symmetry²⁴. A convenient, albeit not unique choice for the order parameter structure of the polar state is $\psi_{-1} = \psi_1, \psi_0 = 0$. The MI lobes, on the other hand, can be classified in two categories: those that correspond to an odd number $n = \sum_i \langle \hat{n}_i \rangle / N$ of bosons per site (here, N is the number of sites), which combine to form a spin-1 object on each site, and lobes in which each site has a 0-spin even n combination. Generically, the even-numbered lobes are more stable and tend to occupy a larger fraction of the μ versus t phase diagram as compared to the nearby odd-numbered lobes, which are smaller and disappear altogether for $U_2/U_0 \geq 0.5$. In addition, for $U_2/U_0 < r_c \approx 0.2$ the even-numbered MI-SF quantum phase transition is first order in character, as opposed to the odd-numbered one which is always continuous. For $U_2/U_0 \geq r_c$, all MI-SF transitions are continuous^{26,27,32}. Finally, the MI is characterized by a vanishing compressibility $\kappa = \partial n / \partial \mu$, which in contrast remains non-zero in the SF.

Once disorder is turned on, a new phase appears: the Bose glass (BG)^{14,32}. The latter is not a SF and therefore the order parameter is zero for any value of α . More precisely, since $\psi_{i\alpha}$ becomes a random quantity in the disordered system, its distribution is given by $P_{\alpha}(\psi_{\alpha}) = \delta(\psi_{\alpha})$ for any α . However, unlike the MI phase, the charge excitation spectrum is gapless and the fluid is compressible: $\partial n / \partial \mu \neq 0$. A full specification of all phases thus requires the computation of the order parameter distribution and the compressibility. It should be noted that there was a long-standing controversy over whether the topology of the phase diagram is such as to allow a direct transition from a MI to a SF, without passing through an intervening BG phase. Scaling arguments suggested that such a direct MI-SF transition is unlikely in the presence of disorder¹⁴. However, numerical results proved to be inconclusive (see, e. g., 29 and 31). More recently, extreme-statistics arguments have been used to show that there are necessarily extended Lifshitz regions of gapless particle-hole excitations at the SF phase boundary³⁶. Therefore, it seems clear now that there is always a BG phase adjacent to the SF and a direct MI-SF is not possible in the disordered case.

III. THE STOCHASTIC MEAN FIELD THEORY

The superfluid-Mott insulator transition of lattice bosons can be qualitatively captured by a standard mean field approach which is based upon decoupling the hopping term of the Hamiltonian (Eq. ((2.7))) as^{14,21,22}

$$a_{i\alpha}^\dagger a_{j\alpha} \simeq \psi_{i\alpha}^* a_{j\alpha} + a_{i\alpha}^\dagger \psi_{j\alpha} - \psi_{i\alpha}^* \psi_{j\alpha}, \quad (3.1)$$

where $\psi_{i\alpha} = \langle a_{i\alpha} \rangle$ and we are neglecting second-order fluctuations $\mathcal{O}(a_{j\alpha} - \langle a_{j\alpha} \rangle)^2$. The order parameters $\psi_{i\alpha}$ have to be determined self-consistently. This is achieved by focusing on the decoupled single-site Hamiltonians generated after (3.1) is applied to (2.7)

$$h_i = - \sum_{\alpha} \left(\eta_{i\alpha} a_{i\alpha}^\dagger + \eta_{i\alpha}^* a_{i\alpha} - \psi_{i\alpha} \eta_{i\alpha}^* \right) + (\epsilon_i - \mu) n_i + \frac{U_0}{2} n_i (n_i - 1) + \frac{U_2}{2} (\mathbf{S}_i^2 - 2n_i), \quad (3.2)$$

where

$$\eta_{i\alpha} = t \sum_{j=1}^Z \psi_{j\alpha}, \quad (3.3)$$

where Z is the lattice coordination number. Once $\langle a_{i\alpha} \rangle (\epsilon_i, \{\psi_{j\beta}\})$ is determined from (3.2) (note the dependence on the local site energy ϵ_i and adjacent order parameters $\psi_{j\alpha}$), self-consistency is assured if we impose that

$$\psi_{i\alpha} = \langle a_{i\alpha} \rangle (\epsilon_i, \{\psi_{j\beta}\}). \quad (3.4)$$

Complete lattice self-consistency requires solving the large set of coupled equations defined by Eqs. (3.4). A considerable simplification can be achieved if we neglect *spatial correlations* between sites. This defines the so-called *stochastic mean field theory* (SMFT) of references 34 and 35, which was originally proposed for the spin-0 model, but which we will now describe for the generic spinful case. For this, we note that $\langle a_{i\alpha} \rangle$ depends on the other order parameters only through $\eta_{i\alpha}$, see Eq. (3.2). We thus look for the distributions of local order parameters $P_\alpha(\psi_\alpha)$ by first finding the distributions of $\eta_{i\alpha}$, $Q_\alpha(\eta_\alpha)$, which are induced by $P_\alpha(\psi_\alpha)$ through Eq. (3.3), *neglecting spatial correlations between different nearest neighbors*. Next, we use the fixed function $\langle a_{i\alpha} \rangle (\epsilon_i, \eta_{i\alpha})$, which usually has to be obtained numerically, to generate the induced distributions $A_\alpha(\langle a_{i\alpha} \rangle)$. Finally, self-consistency is obtained by imposing that $A_\alpha(x) = P_\alpha(x)$. Despite its approximate nature, this approach has been shown to be able to capture all the phases of the spin-0 model^{34,35}.

The procedure described above for the SMFT can be implemented as a non-linear integral equation for the sought distributions $P_\alpha(\psi_\alpha)$, which can then be solved numerically on a discrete mesh. This was the approach

used in references 34 and 35. We opted instead to use an importance sampling method, akin to the Monte Carlo method, as originally proposed for the self-consistent theory of localization^{42,43}. The method can be described as follows. We start from a sample of random values for $\psi_{i\alpha}^{(0)}$ ($i = 1, \dots, N_s$) which are drawn from an initial guess for the sought distributions, $P_\alpha^{(0)}(\psi_\alpha)$. The method is very robust with respect to the choice of this initial guess, so we can start with a uniform distribution. From this initial sample, we generate a corresponding initial sample for $\eta_{i\alpha}$ ($i = 1, \dots, N_s/Z$) using Eq. (3.3), which may be viewed as an initial guess $Q_\alpha^{(0)}(\eta_\alpha)$. Using the latter and a corresponding sample of N_s/Z values of ϵ_i drawn from its (given) distribution, we can then find (numerically solving for $\langle a_{i\alpha} \rangle$ according to (3.2)) a new sample of values of the order parameter $\psi_{i\alpha}^{(1)}$ ($i = 1, \dots, N_s/Z$), which can be viewed as drawn from an improved distribution $P_\alpha^{(1)}(\psi_\alpha)$. The sample size will have decreased by a factor of $1/Z$ from the previous iteration. For further iterations, we can enlarge this smaller sample to the original size by replicating it Z times and reshuffling it. For a large enough value of N_s this leads to negligible errors, which can be checked by studying the dependence of the final results on N_s . The procedure can then be iterated many times until sample-to-sample variations are negligible, which can be verified, for example, by computing sample features such as its mean and variance. A numerical estimate of the converged distribution is then obtained from a histogram of the last several iterations. Furthermore, histograms of any local quantities can also be easily generated.

We have compared the two different methods of solving the SMFT equations, namely, the stochastic method proposed in this paper and the direct solution of the integral equation used in references 34 and 35, in the spin zero case. In Fig. 1, we show a typical result for the order parameter distribution $P(\psi)$ obtained by these two methods, within the disordered Bose-Einstein condensed phase of the spin zero disordered Hubbard model. The importance sampling approach used $N_s = 360,000$ and it took 30 iterations for the convergence to be achieved, after which 70 more iterations were obtained to generate the final statistics. The agreement is remarkable and makes us confident that the method is reliable. In fact, we achieved enough accuracy with $N_s = 60,000$, 40 iterations before convergence and 60 more to gather enough statistics.

Finally, we should mention that the direct computation of the compressibility within SMFT points to a direct transition between the MI and the SF at weak disorder^{34,35}, which is at odds with the rigorous results of 36. The SMFT is thus incapable of capturing the rare regions of gapless charge excitations close to the SF phase that preclude such a direct transition. Arguments have been given in 35, showing how to reinterpret the SMFT phase diagram in order to correct for this failure. Nevertheless, it should be kept in mind that the direct

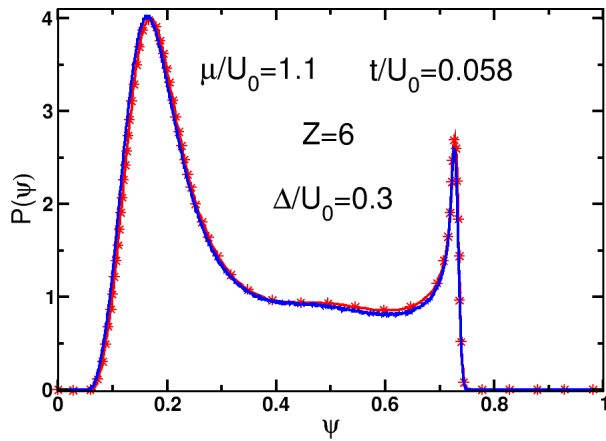


Figure 1. (Color online) Order parameter distribution for the spin zero disordered Hubbard model inside the Bose-Einstein condensed phase obtained within SMFT for $\mu/U_0 = 1.1$, $t/U_0 = 0.058$, $\Delta/U_0 = 0.3$, and $Z = 6$. The full blue line was obtained with the importance sampling method used in this paper and the symbols come from solving directly the integral equation (extracted from reference 44).

calculation of κ does not show the expected behavior.

In the next Section, we will show the results of the SMFT as applied to the disordered spin-1 model of Eq. (2.1).

IV. RESULTS

We now present the results of applying the SMFT to the spin-1 model of Eq. (2.1) at $T = 0$. In all the following results, we have fixed the spin-dependent interaction coupling to be antiferromagnetic with $U_2/U_0 = 0.3$ and $Z = 4$. In Sections IV A to IV E we fix the disorder strength at $\Delta/U_0 = 0.3$. In Section IV F, we study the behavior of the system at fixed μ and t as a function of the disorder.

A. Order parameter

We focus first on the behavior of the order parameter. The clean polar SF phase is characterized by an order parameter structure in which, for a particularly convenient gauge choice, $\psi_{-1} = \psi_1$ and $\psi_0 = 0$ ²¹. This phase corresponds to a spin-zero condensate, as can be easily checked. Fig. 2(a) shows the value of ψ_1 as a color scale plot in the μ vs t phase diagram. The Mott lobes can be clearly identified and also the fact that the even-numbered ones occupy a much larger portion of the phase diagram. The transition from SF to both types of MI is continuous for this value of U_2/U_0 ³².

We then add disorder ($\Delta/U_0 = 0.3$) within a SMFT treatment. We were able to find only converged solutions with $P_1(x) = P_{-1}(x)$ and $P_0(\psi_0) = \delta(\psi_0)$. In other

words, although the order parameter is now a random quantity, it still preserves the same component structure as in the clean case. We have thus produced a color scale plot of the average value of ψ_1 in the same μ vs t phase diagram, as can be seen in Fig. 2(b). This can be viewed as an order parameter for the SF phase in the disordered system. The transitions remain continuous within our accuracy. The boundaries of the Mott lobes of the clean case are shown as black dotted lines for comparison. There is a clear suppression of the regions with a vanishing order parameter (blue regions), except at the wedges that separate the clean Mott lobes, where superfluid order is suppressed. A definite characterization of the non-superfluid regions will be carried out later, when we show the results for the compressibility in Section IV B. We anticipate that the large even-numbered lobes will retain their Mott insulating character. There is a clear suppression of these lobes by disorder, which are seen to become narrower and to extend up to smaller maximum values of the hopping amplitude as compared to the clean case. In contrast, the odd-numbered lobes will be shown to have transformed into the BG phase with a finite compressibility. Their shape is completely deformed by disorder. The conclusion is that the even-numbered MI lobes are more resilient to the effects of disorder. Just like in the clean case, the positive value of U_2 , which stabilizes the even occupation, also acts to localize the bosons more strongly, thus protecting the MI phase against weak disorder. Finally, the small hopping SF wedges that exist between the MI lobes in the clean system are also suppressed by disorder and go into the BG phase.

The full distribution functions $P_1(\psi_1)$ are shown in Fig. 3 for two different values of the chemical potential and several values of the hopping amplitude (again $\Delta/U_0 = 0.3$). In Fig. 3(a), the value of the chemical potential is $\mu/U_0 = 0.1$, which corresponds to the $n = 1$ MI lobe in the clean case at small t . As t is decreased the disordered system goes from a polar SF to a BG phase. It is interesting to note that the distribution is fairly narrow deep in the SF and become increasingly broader and distorted as t decreases, while at the same time its weight shifts towards small values of ψ_1 . In particular, for values of t close to the BG (see, e. g., $t/U_0 = 0.015$ and 0.01), the distribution shows a very skewed shape with a peak at an increasingly smaller ψ_1 and a long tail for larger values of the order parameter. Eventually, it tends towards a delta function at $\psi_1 = 0$ inside the BG phase, barely visible on the scale of the figure at $t/U_0 = 0.005$. This generic behavior is also observed in the SF to BG transition of the spin-zero model³⁴.

In Fig. 3(b), the chemical potential is set to $\mu/U_0 = 1.0$, which in the clean system gives rise to the $n = 2$ MI lobe at small t . As we add disorder, the system can be tuned from the SF to a disordered MI phase. The order parameter distribution shows a markedly different behavior when compared to the $\mu/U_0 = 0.1$ case. Indeed, it retains a fairly narrow shape as t is decreased, while

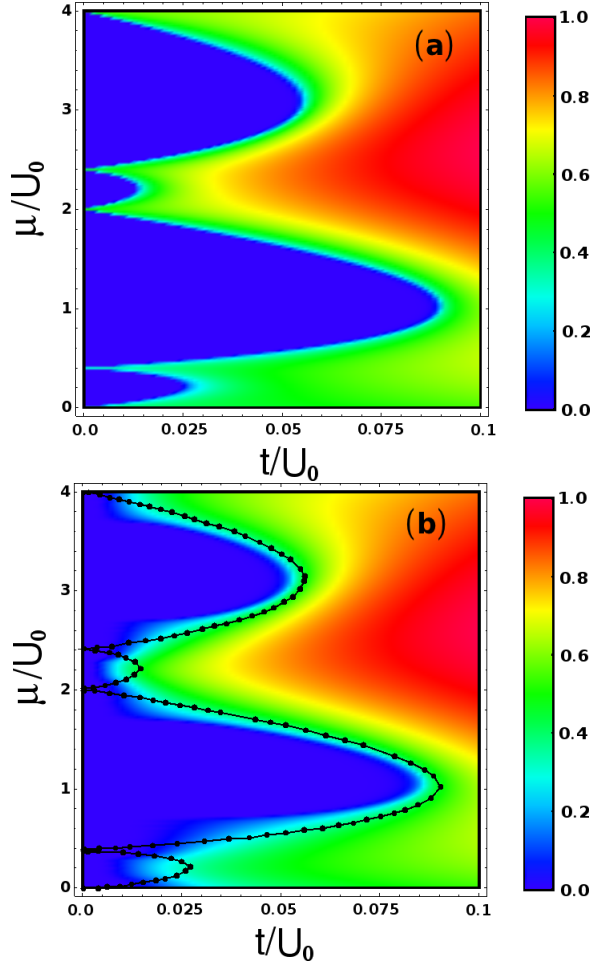


Figure 2. (Color online) Average value of the ψ_1 component of the order parameter in the (t, μ) plane for the (a) clean and (b) disordered ($\Delta/U_0 = 0.3$) cases. In (b) the boundaries of the clean Mott lobes of (a) are shown as black dotted lines.

shifting its weight to ever smaller values of ψ_1 , eventually tending to a delta function at zero within the MI lobe.

B. Compressibility

As was mentioned before, it is essential to analyze the behavior of the compressibility $\kappa = \frac{\partial n}{\partial \mu}$ in order to obtain a complete characterization of the phases: this quantity is finite in both the SF and the BG phases but vanishes in the MI¹⁴.

Fig. 4 shows κ in the μ vs t plane using a color scale for both the clean and disordered cases ($\Delta/U_0 = 0.3$). In the clean case (Fig. 4(a)), the compressibility is zero inside the MI lobes and non-zero in the SF phase. Note that, as $t \rightarrow 0$, the SF phase disappears and the MI lobes are characterized by integer site occupancies, the latter then giving rise to a series of steps of increasing value as μ increases. As a result, the compressibility diverges as

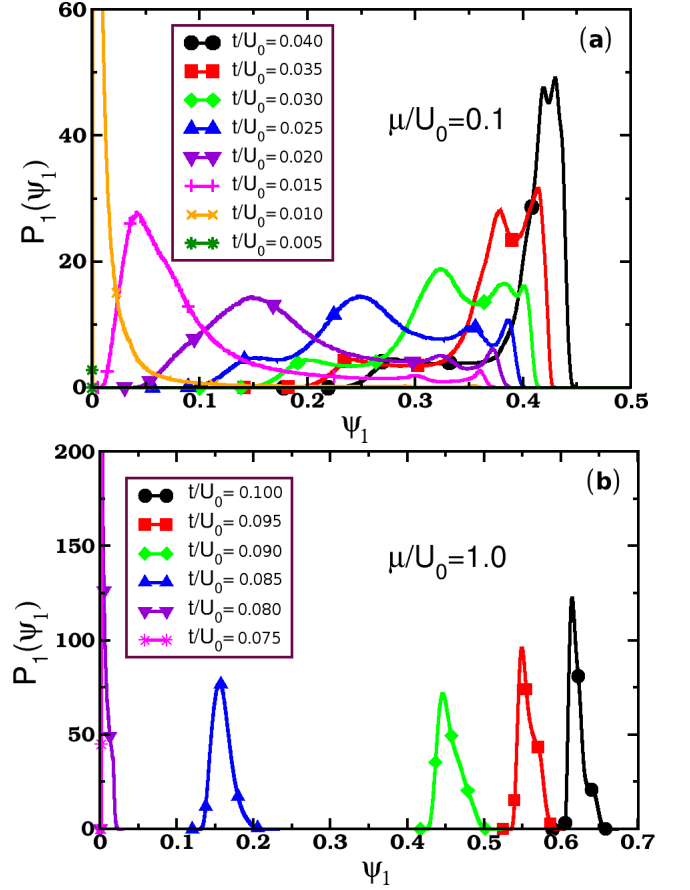


Figure 3. (Color online) Probability distributions for the components of the order parameter $P_1(\psi_1)$ for several values of the hopping amplitude and two values of the chemical potential: (a) $\mu/U_0 = 0.1$ and (b) $\mu/U_0 = 1.0$. The disorder is set to $\Delta/U_0 = 0.3$. As t decreases, the system goes from a disordered polar SF to a BG in (a) and to a MI in (b).

one crosses from one lobe to the next at the $t = 0$ line, since there is a jump in n . Therefore, large values of κ cluster around these transitions in the small t region (red color in the figure). In that figure, we have arbitrarily set $\kappa = 4.22$ to compressibilities equal to or greater than this value.

The compressibility of the disordered system is shown in Fig. 4(b). The regions with zero order parameter from Fig. 2(b) have been delineated as the dotted lines. As can be seen, the compressibility remains zero in large portions of the phase diagram. These regions thus have both vanishing compressibility and order parameter and correspond to even-numbered MI lobes, cf. Fig. 2. Thus, as in the case of the spin-zero model^{34,35}, the SMFT predicts a direct MI-SF transition at this value of disorder, which is an artifact of the approximation used³⁶.

In contrast, however, the small regions which were the odd-numbered MI lobes in the clean case now exhibit a non-zero κ once disorder is added. In other words, these clean MIs are completely destroyed by this amount of randomness and become BGs. It should be said that even

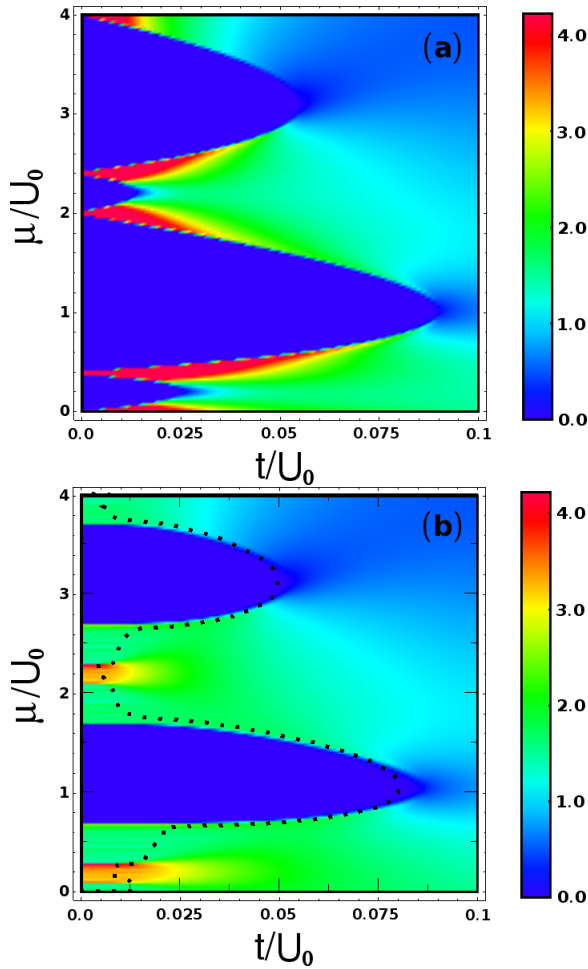


Figure 4. (Color online) Compressibility in the (t, μ) phase diagram. (a) Clean case and (b) disordered case ($\Delta/U_0 = 0.3$). The dotted line delineates the regions characterized by a vanishing order parameter (see Fig. 2(b))

within the SF phase the compressibility can become very small (blueish regions), even though it remains non-zero everywhere in the SF.

Fig. 5 shows some compressibility scans as functions of μ for fixed values of t ; in other words, they correspond to vertical lines in Fig. 4. In the clean case (Fig. 5(a)), the MI regions are clearly demarcated by the vanishing compressibility. Note the large values of κ between MI lobes for $t/U_0 = 0.00625$. Note also that the small odd-numbered MI lobes can only be seen for this smallest value of hopping amplitude.

The addition of disorder with strength $\Delta/U_0 = 0.3$ is enough to completely wipe out the odd-numbered MI lobes, as can be seen in Fig. 5(b). Indeed, it is clear that the compressibility at $t/U_0 = 0.00625$ (blue curves), which vanishes in extended regions around $\mu/U_0 = 0.2$ and 2.2 in Fig. 5(a), becomes non-zero in the same regions after disorder is added, see Fig. 5(b). In fact, it becomes even greater than in the adjacent regions! For the larger values of hopping shown ($t/U_0 = 0.0375, 0.075$),

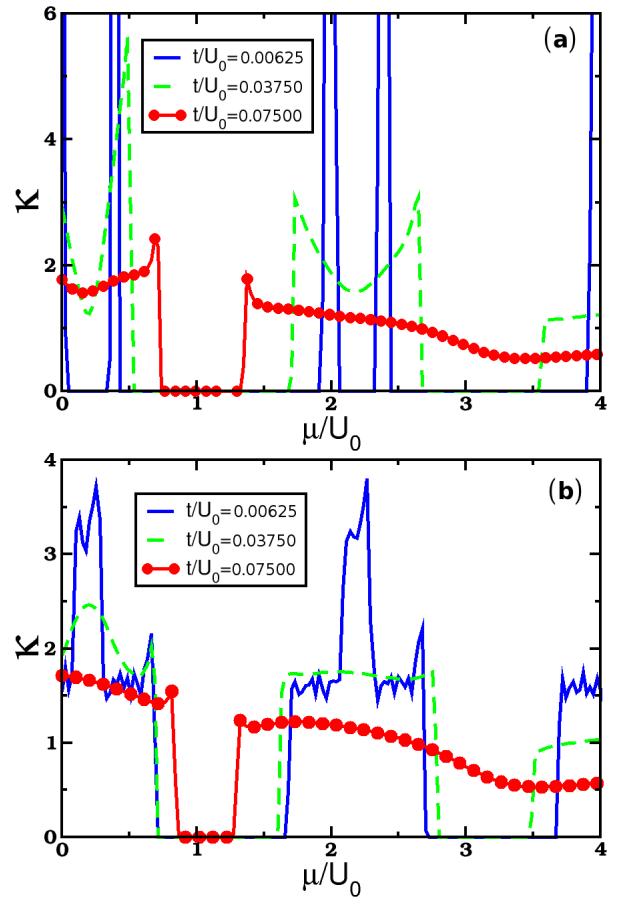


Figure 5. (Color online) The compressibility as a function of the chemical potential for several values of the hopping amplitude: (a) clean case and (b) disordered case ($\Delta/U_0 = 0.3$).

the system is never in the BG phase (cf. Fig. 2(b)) and wherever $\kappa \neq 0$ the system is a SF. It is also noteworthy that the MI lobes that survive have their sizes reduced when compared with the disorder-free case.

In order to further illustrate the joint behavior of the order parameter and the compressibility for fixed disorder ($\Delta/U_0 = 0.3$), we have plotted both quantities together in Fig. 6 as functions of the chemical potential for two different values of the hopping amplitude: (a) $t/U_0 = 0.00125$ and (b) $t/U_0 = 0.00625$. In Fig. 6(a), the SF phase is never stable and the order parameter vanishes for all values of the chemical potential. However, the compressibility is non-zero in large portions of the figure, signaling the BG phase. In Fig. 6(b), by contrast, the SF phase emerges out of the regions of enhanced compressibility. These correspond to the reddish yellow portions of Fig. 4(b).

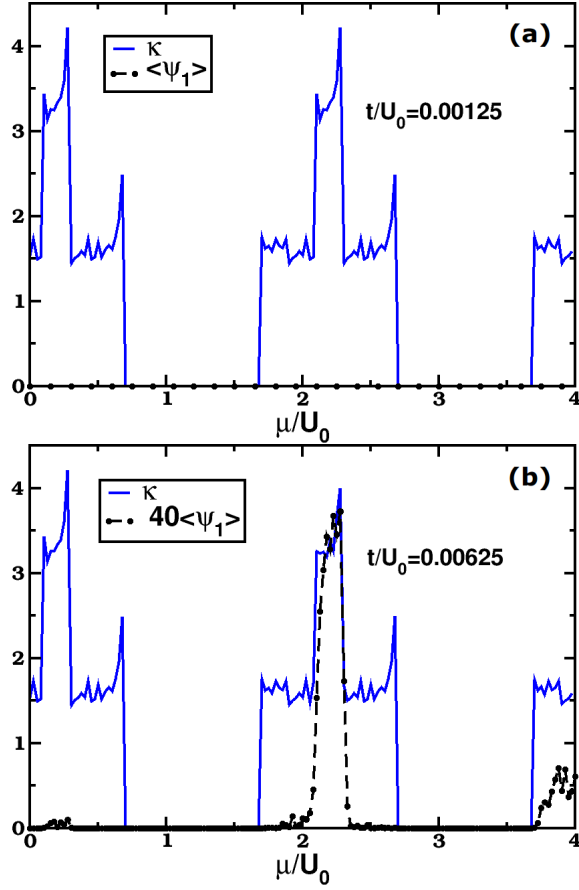


Figure 6. (Color online) The compressibility κ and the average order parameter $\langle\psi_1\rangle$ as functions of the chemical potential for (a) $t/U_0 = 0.00125$ and (b) $t/U_0 = 0.00625$ ($\Delta/U_0 = 0.3$).

C. Condensate fraction

The condensate fraction within SMFT is given by⁴⁴

$$\rho_C = \frac{\sum_{\alpha} |\psi_{\alpha}|^2}{n}, \quad (4.1)$$

which also serves as an order parameter for the MI-SF phase transition. This quantity is shown for both the clean and the disordered (with $\Delta/U_0 = 0.3$) systems in Fig. 7. The behavior in both cases is not qualitatively different from the average order parameter of Fig. 2, as expected.

D. The statistics of the occupation

The site occupation number operator \hat{n}_i is a very useful tool for the characterization of the zero-temperature phases of the clean spin-zero Bose-Hubbard model. Indeed, in the extremely localized MI limit $t \rightarrow 0$, the wave function factorizes into uncorrelated eigenfunctions of \hat{n}_i on each site. In this case, the average occupation

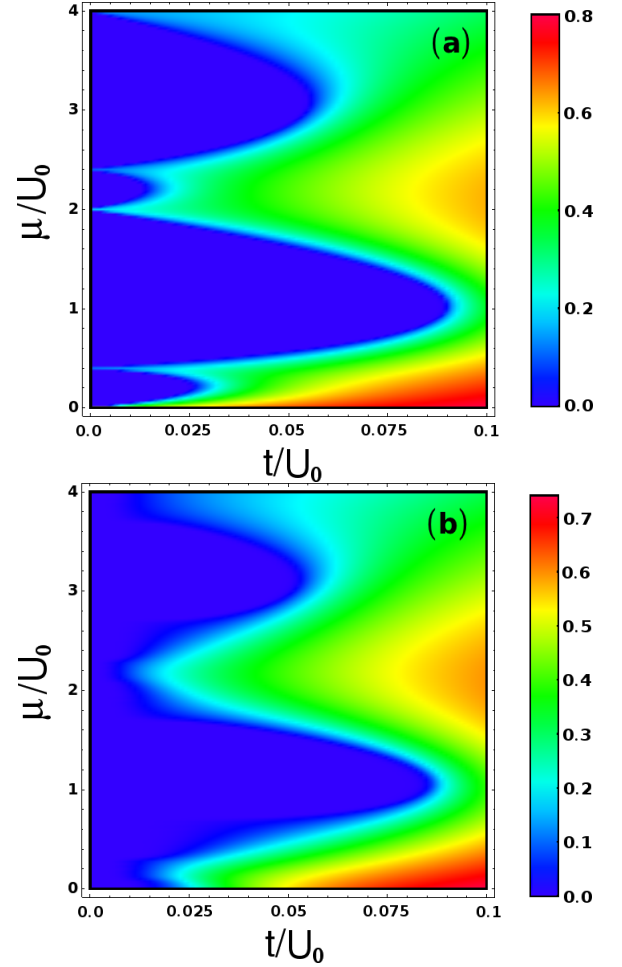


Figure 7. (Color online) The condensate fraction ρ_C for the (a) clean and (b) disordered (with $\Delta/U_0 = 0.3$) cases.

$n_i = \langle\hat{n}_i\rangle$ equals one of the integer eigenvalues and quantum fluctuations of the occupation, as measured by the standard deviation

$$\Delta n_i = \sqrt{\langle\hat{n}_i^2\rangle - \langle\hat{n}_i\rangle^2}, \quad (4.2)$$

are evidently zero. On the other hand, in the other extreme limit of a weakly correlated SF $U \rightarrow 0$, the site occupation number operator is not a good quantum number and there are large quantum fluctuations signaled by a non-zero Δn_i . In the clean case, lattice translation invariance guarantees that both n_i and Δn_i are uniform and do not depend on the site i . Once disorder is added, however, spatial fluctuations of both quantities arise, in addition to the quantum fluctuations already present in the clean system.

A useful measure of these fluctuations is afforded by the distribution function $P_n(n_i)$ and $P_{\Delta n}(\Delta n_i)$, which are both very easily obtained within SMFT from the solutions of the ensemble of single-site Hamiltonians of Eq. (3.2). We will thus now show our results for these distributions for the disordered spin-1 Bose-Hubbard model.

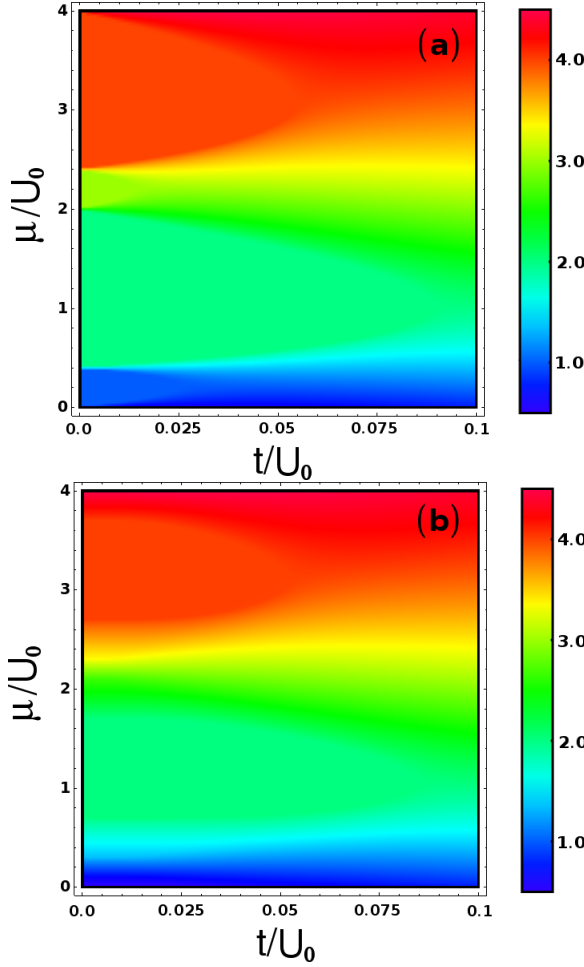


Figure 8. (Color online) The average site occupation number n for the (a) clean and (b) disordered ($\Delta/U_0 = 0.3$) cases in the μ vs t plane.

We start by looking at the spatial average of n_i , which gives the average number of bosons per site n . The two figures can hardly be distinguished, although tiny distortions can be seen. The value of n is useful if we want to assign an integer to the MI lobe, but it is not very useful for a precise demarkation of the phases. However, as we will see, in contrast to the average n the full statistics of n_i imparts a great deal of useful information.

In Fig. 9 $P_n(n_i)$ is shown for two values of chemical potential, $\mu/U_0 = 0.1$ (Fig. 9(a)) and $\mu/U_0 = 1$ (Fig. 9(b)), and for various values of t/U_0 . In Fig. 9(a), the system goes from a SF to a BG as the hopping decreases. The spatial fluctuations of n_i are large in both phases. As the hopping decreases and the system approaches the BG phase, the distribution function acquires a bimodal shape, with increasingly sharper peaks around $n_i = 0$ and $n_i = 1$ and decreasing weight in the region between these two values. Inside the BG phase ($t/U_0 = 0.01$ and 0.005), the peak around $n_i = 0$ becomes a delta function while the peak at $n_i = 1$ remains broad. This spatial landscape in which different sites are Mott localized at

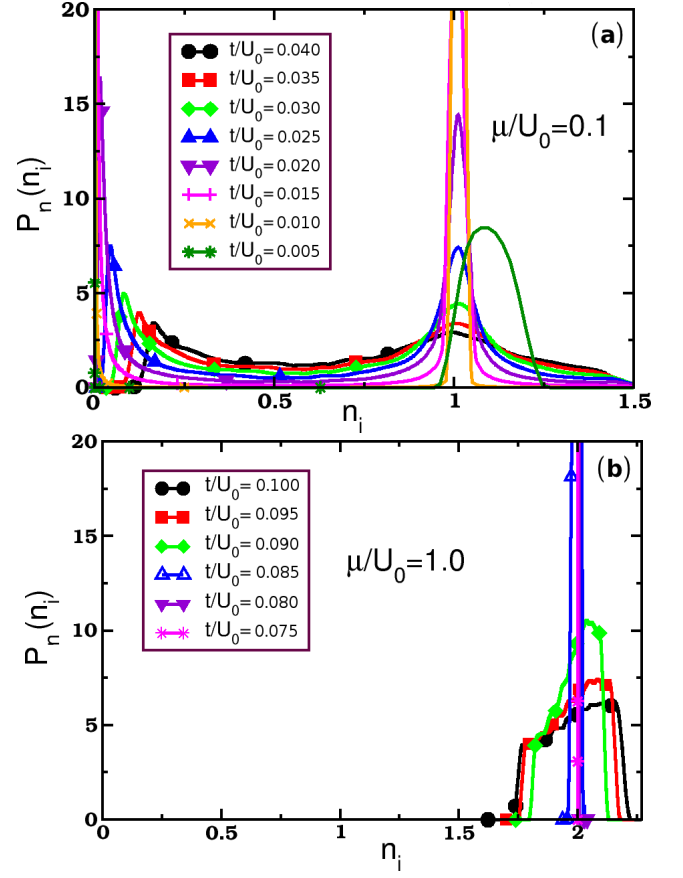


Figure 9. (Color online) The probability distribution functions of the average site occupation number $P_n(n_i)$ for (a) $\mu/U_0 = 0.1$, and (b) $\mu/U_0 = 1$ and various values of the hopping amplitude. In (a) the system goes through the SF-BG transition and in (b) from SF to MI, as the hopping amplitude decreases. The disorder is set to $\Delta/U_0 = 0.3$.

different occupations is characteristic of the BG phase¹⁴ and is vividly illustrated by $P_n(n_i)$.

The behavior observed across the SF-MI phase transition is markedly different, as can be seen in Fig. 9(b). In this case, $P_n(n_i)$ starts as a mildly broad distribution around $n_i = 2$ in the SF, which becomes increasingly narrower as the hopping is reduced and the system transitions into the MI phase. Inside the MI lobe ($t/U_0 = 0.08$ and 0.075), the distribution becomes a delta function centered at $n_i = 2$, showing that in the disordered MI the system is locked at a fixed unique occupation.

We now turn to the spatial fluctuations of Δn_i as measured by $P_{\Delta n}(\Delta n_i)$. We start by looking at the spatial average of Δn_i in Fig. 10. Within SMFT, both MI and BG phases are characterized by the vanishing of the order parameter $\psi_{i\alpha}$ and thus of the $\eta_{i\alpha}$ field that acts on each site, see Eqs. (3.3) and (3.2). If $\eta_{i\alpha}$ is zero, the ground state of every site is an eigenvector of the number operator and, therefore, $\Delta n_i = 0$ for all sites. This is why the average Δn_i is also zero within both the MI and the BG phases. This is a feature of the mean field character of

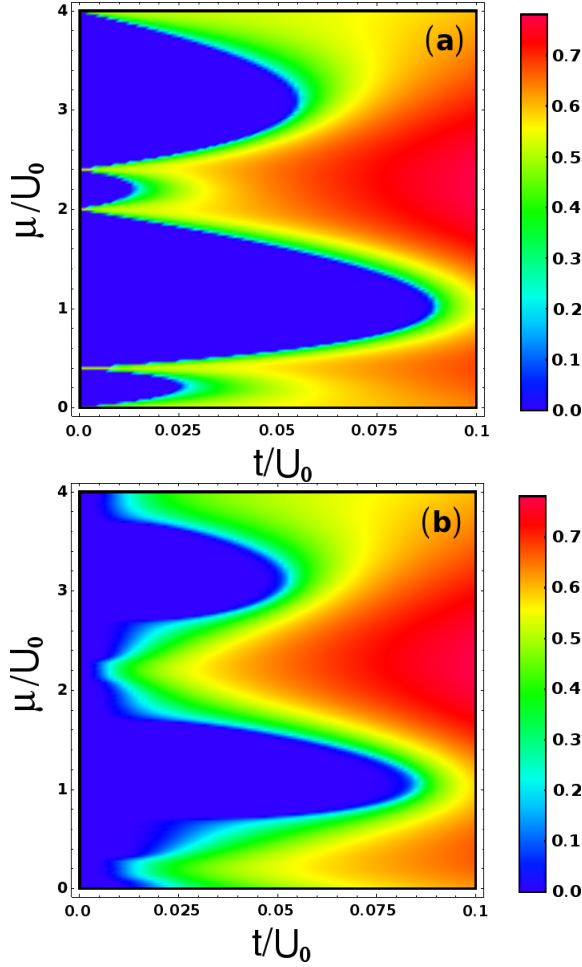


Figure 10. (Color online) Spatial average of the site occupation standard deviation Δn_i in the μ vs t plane: (a) clean and (b) disordered ($\Delta/U_0 = 0.3$) cases.

the theory and is not expected to survive beyond this approximation. In contrast, $\Delta n_i \neq 0$ everywhere in the SF phase and so is its average, making it an alternative order parameter for that phase in the clean as well as in the disordered cases. Note that, although in the BG phase $\Delta n_i = 0$ at every site and there are no quantum fluctuations of the site occupation (within SMFT), the average site occupation does exhibit large spatial fluctuations, as was already seen in Fig. (9)(a).

The full distributions $P_{\Delta n}(\Delta n_i)$ are shown in Fig. 11 for the two chemical potential values $\mu/U_0 = 0.1$ and 1.0 that allow us to study the SF to BG and MI phase transitions. In the first case (Fig. 11(a)), the distribution is mildly broad, approximately bimodal and with support around $\Delta n_i \approx 0.5$ in the SF. As t decreases and the system approaches the BG, the distribution widens with a small and sharp peak at ≈ 0.5 and a broader one centered at a lower value which slowly shifts towards zero while at the same time gaining more weight. Eventually, in the BG phase, the distribution degenerates into a delta function at zero, consistent with the vanishing average value

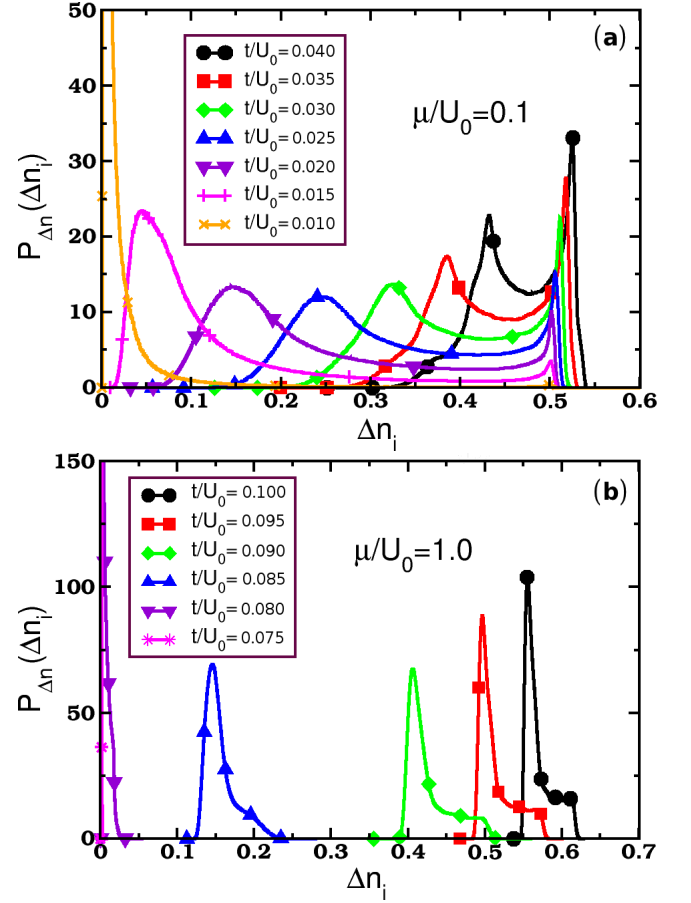


Figure 11. (Color online) Probability distributions of the site occupation standard deviation Δn_i for two values of the chemical potential: (a) $\mu/U_0 = 0.1$ (corresponding to the SF to BG transition) and (b) $\mu/U_0 = 1.0$ (which corresponds to the transition from SF to MI), for various values of the hopping amplitude and for fixed disorder strength $\Delta/U_0 = 0.3$.

found before.

Finally, the behavior of $P_{\Delta n}(\Delta n_i)$ for the SF to MI transition case is shown in Fig. 11(b). The behavior is now distinctively different: the distributions are always confined to a small region of support, whose center shifts towards zero and whose width decreases as the system enters the MI phase. As discussed before, the presence of local occupation number quantum fluctuations is intimately tied to the non-zero value of $\eta_{i\alpha}$. Therefore, it should not be viewed as too surprising that the qualitative behavior of $P_{\Delta n}(\Delta n_i)$ closely follows that of $P_1(\psi_1)$, cf. Figs. 3 and 11.

E. Spin

Another quantity of importance in the characterization of the phases is the average square of the total spin of each site $\langle S_i^2 \rangle \equiv S_i^2$. In the clean limit, this quantity is zero in the even-numbered MI lobes, since the bosons

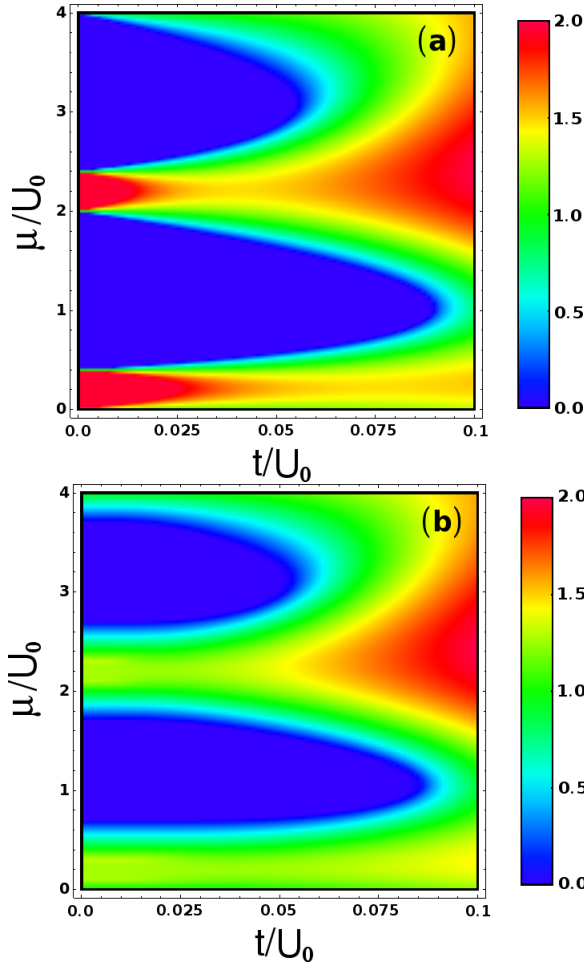


Figure 12. (Color online) The spatial average of the mean square of the total spin per site $\langle S_i^2 \rangle$: (a) clean and (b) disordered ($\Delta/U_0 = 0.3$) cases.

are able to combine into a zero-spin composite at each site thus decreasing the spin-dependent interaction contribution to the total energy. In contrast, it is impossible to do so when there is an odd number of bosons per site and the best compromise to lower the energy is to form a spin-1 combination, in which case $S_i^2 = 2$. This situation is depicted in Fig. 12(a). Interestingly, the polar SF is characterized in general by intermediate values of this quantity, with a tendency towards saturation to $S_i^2 = 2$ when the hopping is large and the SF well formed. It should be noted that inter-site spin correlations, absent in the mean-field treatment used here, are able to generate complex spin arrangements in the ground state. In particular, spin nematic order is predicted to occur throughout the odd-numbered MI lobes and in part of the even-numbered ones²⁸. This type of order is characterized by broken spin rotational invariance ($\langle (S_i^a)^2 \rangle \neq 0$, $a = x, y$ or z) accompanied by unbroken time reversal symmetry ($\langle \mathbf{S}_i \rangle = 0$).

The most dramatic effect of the introduction of disorder

is seen in the BG phase, see Fig. 12(b). In that case, the presence of sites with different average occupations, both even and odd (see Fig. 9(a)), leads to the settling of the spatial average of S_i^2 at a value intermediate between 0 and 2. There is actually a very smooth dependence of this spatial average on t as we move from the SF into the BG phase. In the MI phase, on the other hand, the spatial average of S_i^2 still vanishes and in the SF it also retains its generic intermediate values.

The probability distribution of the expectation value of the square of the total spin per site $P_{S^2}(S_i^2)$ is shown in Fig. 13 for the two values of $\mu/U_0 = 0.1$ and 1.0 and several values of the hopping amplitude. From the previous discussion, the behavior of $P_{S^2}(S_i^2)$ is expected to track closely the distribution of the average site occupation $P_n(n_i)$. Indeed, upon approaching the BG from the SF as t decreases, as shown in Fig. 13(a), the distribution of S_i^2 becomes increasingly broader with a bimodal shape, indicating the gradual appearance of both spin-zero and spin-1 sites, corresponding to the peaks at $n_i = 0$ and $n_i = 1$, respectively, of Fig. 9(a). Likewise, as t decreases and the system transitions from the SF to the MI, as depicted in Fig. 13(b), the S_i^2 distribution shifts weight from non-zero values spread around ≈ 1 down to a delta function at zero, at the same time as the average occupation distribution narrows down to a delta function at occupation $n_i = 2$.

It was argued in reference 32 that the *spatially-averaged* value of $\langle S_i^2 \rangle$ intermediate between 0 and 2 of the BG phase shown in Fig. 12(b) is indicative of a spin nematic phase²⁸. In the clean case discussed in 28, however, it is quantum inter-site spin correlations that are responsible for the appearance of nematic order. This occurs even at perturbatively small t , in which case each site has a fixed odd number of bosons. On the other hand, no inter-site spin correlations are incorporated in the SMFT and the BG phase is characterized by the presence of sites with different number occupations, see Fig. 9(a). It is these sites, with an odd number of bosons and $S_i = 1$ or an even number and $S_i = 0$, which are ultimately responsible for the intermediate value of $\langle S_i^2 \rangle$ which both the SMFT and the Gutzwiller approach of reference 32 find. This situation is rather different from the clean nematic and should not, in our view, be confused with it.

F. The quantum phase transition as a function of disorder

In previous Sections we fixed the disordered strength and analyzed the behavior of the system as a function of the chemical potential and the hopping amplitude. For the value of disorder we used ($\Delta/U_0 = 0.3$), the clean even-numbered MI lobes survived the introduction of randomness, whereas the odd-numbered ones were completely destroyed. It would be interesting to see how the former behave as the disorder strength is further in-

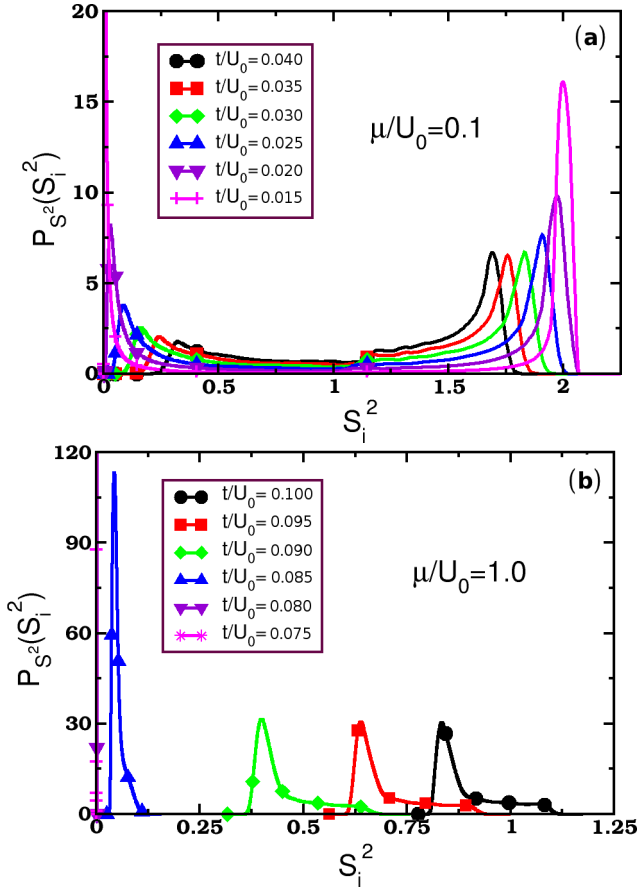


Figure 13. (Color online) The probability distribution functions $P_{S_i^2}(S_i^2)$ of the square of the total spin per site for various values of the hopping amplitude and two values of the chemical potential: (a) $\mu/U_0 = 0.1$ and (b) $\mu/U_0 = 1.0$. The disorder is set to $\Delta/U_0 = 0.3$.

creased. We take up this task in this Section.

We show in Fig. 14 the various distribution functions in the strong disorder regime ($\Delta \geq U_0$) for $\mu/U_0 = 1.0$ and $t/U_0 = 0.075$. We remind the reader that for $\Delta = 0$, this corresponds to a point well inside the $n_i = 2, S_i = 0$ MI lobe. The order parameter distribution $P_1(\psi_1)$ is shown in Fig. 14(a). For $\Delta/U_0 = 1.0$ the MI lobe has been suppressed in favor of the disordered SF phase, characterized by finite SF order parameters. As Δ is increased, this distribution broadens with increasing weight at $\psi_1 = 0$. Eventually, for large enough randomness, the distribution collapses to a delta function at $\psi_1 = 0$, signaling the destruction of the SF phase. The distribution of site occupation standard deviation $P_{\Delta n}(\Delta n_i)$, depicted in Fig. 14(b), shows a qualitatively similar behavior, as expected. As discussed in Section IVD, this quantity largely tracks the distribution of the order parameters. But is the non-SF phase at large values of Δ a BG or a MI?

One possible diagnostics tool is afforded by the distribution of the mean square of the total spin per site, as shown in Fig. 15(a). It shows the typical broad, bi-

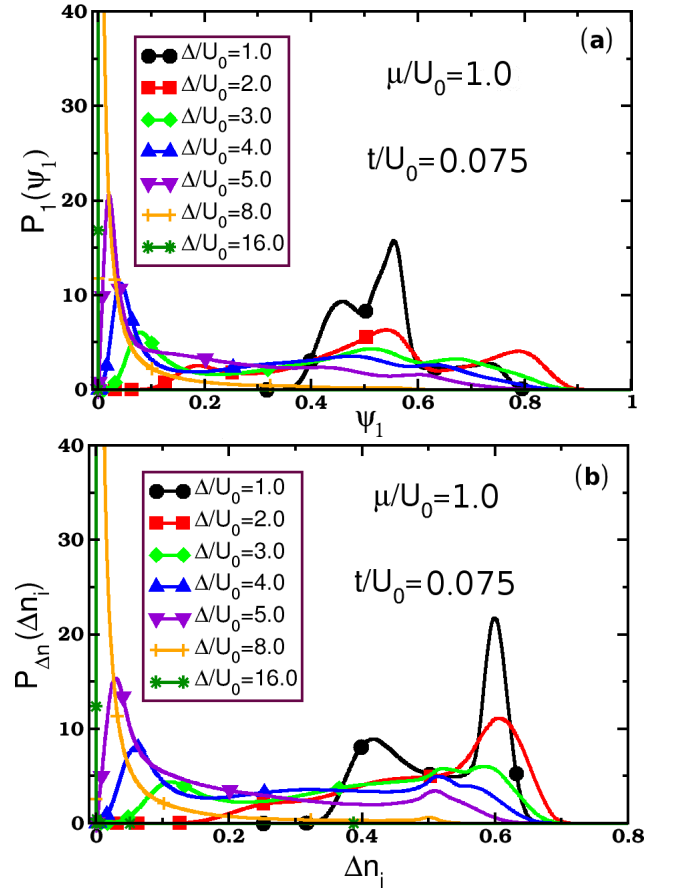


Figure 14. (Color online) Probability distributions functions of: (a) the order parameter and (b) the standard deviation of the occupation, for various values of disorder parameter Δ/U_0 . The chemical potential is fixed at $\mu/U_0 = 1$ and the hopping amplitude at $t/U_0 = 0.075$.

modal shape characteristic of the BG distribution as Δ increases, indicating the presence of both singlet (weight at 0) and spin-1 (weight around 2) composites at each site. This should be compared with the similar small t distributions of Fig. 13(a), characteristic of the BG phase, and contrasted with the corresponding curves of Fig. 13(b), which are associated with MI behavior.

Even more significant is the behavior of the distribution of the average site occupation number $P_n(n_i)$, shown in Fig. 15(b). As Δ increases, it is clearly seen that the distribution gradually evolves into essentially isolated peaks centered around the integer values (1 through 4 for $\Delta/U_0 = 16$). The presence of sites with different integer occupations in a non-SF phase is the hallmark of the BG, cf. Fig. 9(a).

In order to dissipate any doubt that the large disorder phase for this particular choice of parameters is indeed a BG, we show in Fig. 16 the compressibility as a function of disorder strength. Its value decreases with increasing disorder but remains finite at the largest value analyzed ($\Delta/U_0 = 16$) at which point the order parameter has

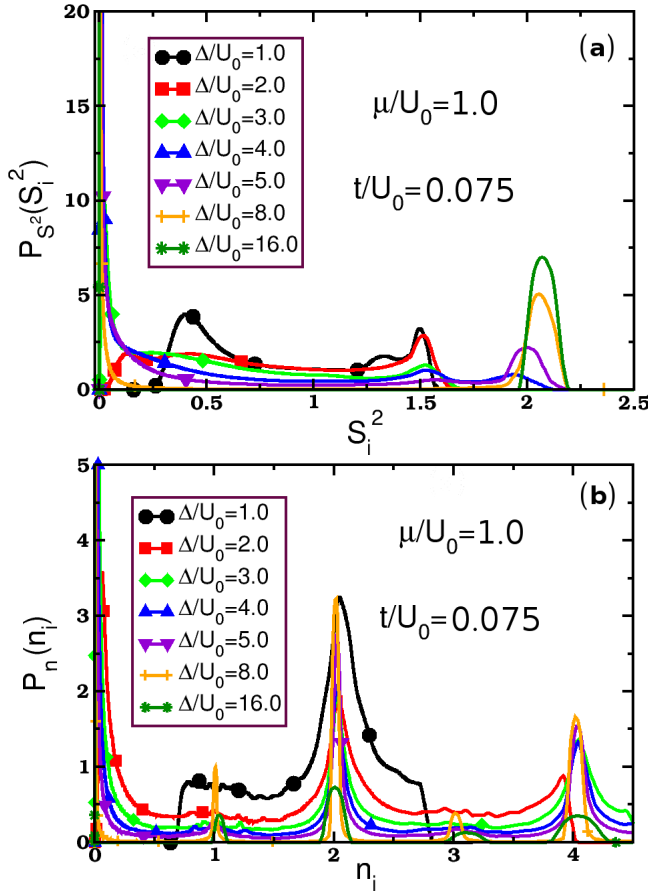


Figure 15. (Color online) Probability distributions functions of: (a) the expectation value of the square of the spin operator per site and (b) the average site occupation number, for various values of disorder parameter Δ/U_0 . The chemical potential is fixed at $\mu/U_0 = 1$ and the hopping amplitude at $t/U_0 = 0.075$.

already vanished, cf. Fig. 14(a).

This shows that, though more robust against randomness, the even-numbered MI lobes can also be wiped out and transformed into BG phases with sufficiently large disorder. It follows that, for large enough values of Δ , only the SF and the BG phases survive, as had been previously observed in the spin-zero case^{34,35}.

V. CONCLUSIONS

We have analyzed the stochastic mean field theory of the disordered spin-1 Bose-Hubbard and discussed its physical properties as a function of the hopping amplitude, the chemical potential and the disorder strength. Although the model exhibits strong similarities with its spin-zero counterpart, several differences stand out. There is a clear difference in the behavior of the odd- and the even-numbered MI lobes. The latter are much more robust with respect to the introduction of disorder. As a result, there is a sizable portion of the parameter

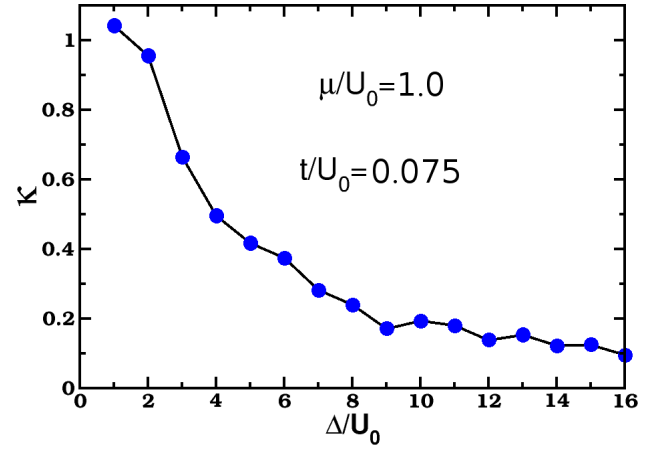


Figure 16. (Color online) The compressibility as a function of disorder strength. The chemical potential is fixed at $\mu/U_0 = 1$ and the hopping amplitude at $t/U_0 = 0.075$.

space in which only even-numbered MI lobes exist, the odd-numbered ones having been transformed into a BG. The BG insulator is characterized by a finite compressibility and the presence of sites with different occupations, like the spin-zero case. However, unlike the spin-zero case, different occupations give rise to different spins. Therefore, the spin-1 BG is an inhomogeneous mixture of spin-0 and spin-1 composites within the SMFT. Very similar behavior was obtained within the Gutzwiller approach of reference 32. We should stress that reference 32 employs two different approaches in the study of the disordered system. In one approach, which the authors call a ‘probabilistic mean-field theory’, only an average order parameter is considered in the description. This approach is a much poorer description than the present SMFT, since it incorporates no spatial fluctuations and, in particular, does not exhibit a BG phase. Alternatively, they also show a direct lattice calculation of the site-decoupled mean-field theory. This does have spatial fluctuations and describes all 3 phases. It includes spatial correlations of the local order parameter which are absent in our SMFT treatment and should therefore be considered a superior approach. However, direct comparison shows that the phase diagram and some physical properties we obtain are almost exactly the same as the lattice calculation of reference 32, highlighting that the much simpler SMFT already incorporates the most important correlations of the more complete treatment.

The presence of local composites with different total spin values raises the important question of the spin correlations within the spin-1 BG phase. As discussed in 28 for the clean system, spin correlations outside the scope of either the ‘site-decoupled’ mean-field theory or the Gutzwiller approach give rise to non-trivial nematic ground states. It would be of great interest to incorporate these into a description of the disordered system in order to investigate the interplay between disorder-induced number fluctuations and quantum inter-site correlations.

Besides the possibility of a spin nematic, the introduction of randomness could also potentially give rise to spin-glass order, a Bose-spin-glass or quantum Griffiths phases^{45–48}.

Another direction deserving of further scrutiny is the case of ferromagnetic interactions, $U_2 < 0$. In this case, we expect the MI lobes to be characterized by the bosons aligning to form a maximum spin composite. In the presence of strong enough disorder, spins of different sizes are expected to form, rendering the problem of the ground

state spin structure even richer.

ACKNOWLEDGMENTS

This work was supported by CNPq through grants 304311/2010-3 (EM) and 140184/2007-4 (JHW) and by FAPESP through grant 07/57630-5 (EM).

- ¹ M. Greiner, O. Mandel, T. Esslinger, T. W. Hansch, and I. Bloch, *Nature* **415**, 0028 (2002).
- ² M. Lewenstein, A. Sanpera, V. Ahufinger, B. Damski, A. S. De, and U. Sen, *Adv. Phys.* **56**, 243 (2007).
- ³ P. Horak, J.-Y. Courtois, and G. Grynberg, *Phys. Rev. A* **58**, 3953 (1998).
- ⁴ D. Boiron, C. Mennerat-Robilliard, J.-M. Fournier, L. Guidoni, C. Salomon, and G. Grynberg, *Eur. Phys. J. D* **7**, 373 (1999).
- ⁵ R. Roth and K. Burnett, *Phys. Rev. A* **68**, 023604 (2003).
- ⁶ B. Damski, J. Zakrzewski, L. Santos, P. Zoller, and M. Lewenstein, *Phys. Rev. Lett.* **91**, 080403 (2003).
- ⁷ R. B. Diener, G. A. Georgakis, J. Zhong, M. Raizen, and Q. Niu, *Phys. Rev. A* **64**, 033416 (2001).
- ⁸ L. Fallani, J. E. Lye, V. Guarrera, C. Fort, and M. Inguscio, *Phys. Rev. Lett.* **98**, 130404 (2007).
- ⁹ E. Lucioni, B. Deissler, L. Tanzi, G. Roati, M. Zaccanti, M. Modugno, M. Larcher, F. Dalfovo, M. Inguscio, and G. Modugno, *Phys. Rev. Lett.* **106**, 230403 (2011).
- ¹⁰ U. Gavish and Y. Castin, *Phys. Rev. Lett.* **95**, 020401 (2005).
- ¹¹ P. Massignan and Y. Castin, *Phys. Rev. A* **74**, 013616 (2006).
- ¹² H. Gimpelrein, S. Wessel, J. Schmiedmayer, and L. Santos, *Phys. Rev. Lett.* **95**, 170401 (2005).
- ¹³ P. A. Lee and T. V. Ramakrishnan, *Rev. Mod. Phys.* **57**, 287 (1985).
- ¹⁴ M. P. A. Fisher, P. B. Weichman, G. Grinstein, and D. S. Fisher, *Phys. Rev. B* **40**, 546 (1989).
- ¹⁵ K. Sheshadri, H. Krishnamurthy, R. Pandit, and T. Ramakrishnan, *Europhys. Lett* **22**, 257 (1993).
- ¹⁶ D. Jaksch, C. Bruder, J. I. Cirac, C. W. Gardiner, and P. Zoller, *Phys. Rev. Lett.* **81**, 3108 (1998).
- ¹⁷ T.-L. Ho, *Phys. Rev. Lett.* **81**, 742 (1998).
- ¹⁸ T. Ohmi and K. Machida, *Journal of the Physical Society of Japan* **67**, 1822 (1998).
- ¹⁹ S. Mukerjee, C. Xu, and J. E. Moore, *Phys. Rev. Lett.* **97**, 120406 (2006).
- ²⁰ M. Ueda, *Annu. Rev. Condens. Matter Phys.* **3**, 263 (2012).
- ²¹ S. Tsuchiya, S. Kurihara, and T. Kimura, *Phys. Rev. A* **70**, 043628 (2004).
- ²² D. van Oosten, P. van der Straten, and H. T. C. Stoof, *Phys. Rev. A* **63**, 053601 (2001).
- ²³ C. N. Yang, *Rev. Mod. Phys.* **34**, 694 (1962).
- ²⁴ E. H. Lieb, R. Seiringer, and J. Yngvason, *Rep. Math. Phys.* **59**, 389 (2007).
- ²⁵ P. Anders, E. Gull, L. Pollet, M. Troyer, and P. Werner, *New J. of Phys.* **13**, 075013 (2011).
- ²⁶ T. Kimura, S. Tsuchiya, and S. Kurihara, *Phys. Rev. Lett.* **94**, 110403 (2005).
- ²⁷ R. V. Pai, K. Sheshadri, and R. Pandit, *Phys. Rev. B* **77**, 014503 (2008).
- ²⁸ A. Imambekov, M. Lukin, and E. Demler, *Phys. Rev. A* **68**, 063602 (2003).
- ²⁹ W. Krauth, N. Trivedi, and D. Ceperley, *Phys. Rev. Lett.* **67**, 2307 (1991).
- ³⁰ S. Rapsch, U. Schollwöck, and W. Zwerger, *Europhys. Lett* **46**, 559 (1999).
- ³¹ N. Prokof'ev and B. Svistunov, *Phys. Rev. Lett.* **92**, 015703 (2004).
- ³² M. Łącki, S. Paganelli, V. Ahufinger, A. Sanpera, and J. Zakrzewski, *Phys. Rev. A* **83**, 013605 (2011).
- ³³ K. Sheshadri, H. R. Krishnamurthy, R. Pandit, and T. V. Ramakrishnan, *Phys. Rev. Lett.* **75**, 4075 (1995).
- ³⁴ U. Bissbort and W. Hofstetter, *EPL* **86**, 50007 (2009).
- ³⁵ U. Bissbort, R. Thomale, and W. Hofstetter, *Phys. Rev. A* **81**, 063643 (2010).
- ³⁶ L. Pollet, N. V. Prokof'ev, B. V. Svistunov, and M. Troyer, *Phys. Rev. Lett.* **103**, 140402 (2009).
- ³⁷ V. Gurarie, L. Pollet, N. V. Prokof'ev, B. Svistunov, and M. Troyer, *Phys. Rev. B* **80**, 214519 (2009).
- ³⁸ E. Altman, Y. Kafri, A. Polkovnikov, and G. Refael, *Phys. Rev. Lett.* **93**, 150402 (2004).
- ³⁹ E. Altman, Y. Kafri, A. Polkovnikov, and G. Refael, *Phys. Rev. Lett.* **100**, 170402 (2008).
- ⁴⁰ E. Altman, Y. Kafri, A. Polkovnikov, and G. Refael, *Phys. Rev. B* **81**, 174528 (2010).
- ⁴¹ S. Iyer, D. Pekker, and G. Refael, *Phys. Rev. B* **85**, 094202 (2012).
- ⁴² R. Abou-Chacra, D. J. Thouless, and P. W. Anderson, *Journal of Physics C: Solid State Physics* **6**, 1734 (1973).
- ⁴³ M. C. O. Aguiar, E. Miranda, and V. Dobrosavljević, *Phys. Rev. B* **68**, 125104 (2003).
- ⁴⁴ U. Bissbort, Diploma thesis, University of Frankfurt (2007), URL http://itp.uni-frankfurt.de/~bissbort/Bissbort_Thesis.pdf.
- ⁴⁵ Y.-C. Lin, R. Mélin, H. Rieger, and F. Iglói, *Phys. Rev. B* **68**, 024424 (2003).
- ⁴⁶ F. Iglói and C. Monthus, *Phys. Rep.* **412**, 277 (2005).
- ⁴⁷ E. Miranda and V. Dobrosavljević, *Rep. Prog. Phys.* **68**, 2337 (2005).
- ⁴⁸ T. Vojta, *J. Phys. A: Math. Gen.* **39**, R143 (2006).